

# Shedding Light on the Enigmatic $\text{TcO}_2 \cdot x\text{H}_2\text{O}$ Structure with Density Functional Theory and EXAFS Spectroscopy\*\*

Augusto F. Oliveira,<sup>\*,[a, b]</sup> Agnieszka Kuc,<sup>[a]</sup> Thomas Heine,<sup>[a, b, c]</sup> Ulrich Abram,<sup>[d]</sup> and Andreas C. Scheinost<sup>\*,[e, f]</sup>

**Abstract:** The  $\beta$ -emitting  $^{99}\text{Tc}$  isotope is a high-yield fission product in  $^{235}\text{U}$  and  $^{239}\text{Pu}$  nuclear reactors, raising special concern in nuclear waste management due to its long half-life and the high mobility of pertechnetate ( $\text{TcO}_4^-$ ). Under the conditions of deep nuclear waste repositories, Tc is retained through biotic and abiotic reduction of  $\text{TcO}_4^-$  to compounds like amorphous  $\text{TcO}_2 \cdot x\text{H}_2\text{O}$  precipitates. It is generally accepted that these precipitates have linear  $(\text{Tc}(\mu\text{-O})_2(\text{H}_2\text{O})_2)_n$  chains, with *trans*  $\text{H}_2\text{O}$ . Although corresponding Tc–Tc and

Tc–O distances have been obtained from extended X-ray absorption fine structure (EXAFS) spectroscopy, this structure is largely based on analogy with other compounds. Here, we combine density-functional theory with EXAFS measurements of fresh and aged samples to show that, instead,  $\text{TcO}_2 \cdot x\text{H}_2\text{O}$  forms zigzag chains that undergo a slow aging process whereby they combine to form longer chains and, later, a tridimensional structure that might lead to a new  $\text{TcO}_2$  polymorph.

## Introduction

Technetium is the lightest element without a stable isotope and is almost completely artificial; only trace amounts are found in nature, formed from spontaneous fission in uranium minerals.

$^{99\text{m}}\text{Tc}$  (metastable) is of great importance in nuclear medicine as a  $\gamma$ -ray emitter,<sup>[1]</sup> while the  $\beta$ -emitting  $^{99}\text{Tc}$  (ground state) has no practical use and raises special concern in nuclear waste management due to its long half-life (ca.  $2.1 \times 10^5$  years) and relatively high formation yield ( $\geq 6\%$ ) in  $^{235}\text{U}$  and  $^{239}\text{Pu}$  nuclear reactors.

[a] Dr. A. F. Oliveira, Dr. A. Kuc, Prof. Dr. T. Heine  
Institute of Resource Ecology  
Helmholtz-Zentrum Dresden-Rossendorf (HZDR)  
Forschungsstelle Leipzig  
Permoserstr. 15, 04318 Leipzig (Germany)  
E-mail: a.faria-oliveira@hzdr.de

[b] Dr. A. F. Oliveira, Prof. Dr. T. Heine  
Theoretische Chemie, Technische Universität Dresden  
Bergstr. 66c, 01062 Dresden (Germany)

[c] Prof. Dr. T. Heine  
Department of Chemistry, Yonsei University  
50 Yonsei-ro, Seodaemun-gu  
Seoul 03722 (Republic of Korea)

[d] Prof. Dr. U. Abram  
Institut für Chemie und Biochemie  
Anorganische Chemie, Freie Universität Berlin  
Fabeckstr. 34–36, 14195 Berlin (Germany)

[e] Dr. A. C. Scheinost  
Institute of Resource Ecology  
Helmholtz-Zentrum Dresden-Rossendorf (HZDR)  
Bautzner Landstr. 400, 01328 Dresden (Germany)

[f] Dr. A. C. Scheinost  
The Rossendorf Beamline (ROBL)  
European Synchrotron Radiation Facility (ESRF)  
71, Avenue des Martyrs, Grenoble 38043 (France)  
E-mail: scheinost@esrf.fr

[\*\*] A previous version of this manuscript has been deposited on a preprint server (<https://doi.org/10.26434/chemrxiv-2022-rjndn>)

Supporting information for this article is available on the WWW under <https://doi.org/10.1002/chem.202202235>

© 2022 The Authors. Chemistry - A European Journal published by Wiley-VCH GmbH. This is an open access article under the terms of the Creative Commons Attribution License, which permits use, distribution and reproduction in any medium, provided the original work is properly cited.

In water and in absence of other complexing agents, Tc prevails in oxidation states VII and IV.<sup>[2]</sup> Under nonreducing conditions,  $\text{Tc}^{\text{VII}}$  forms the soluble  $\text{TcO}_4^-$  anion, which is highly mobile in the environment due to its weak interaction with adsorbent surfaces. Under the reducing conditions of natural, anoxic sediments as well as in nuclear waste repositories, however, numerous studies suggest that Tc precipitates as  $\text{TcO}_2 \cdot x\text{H}_2\text{O}$ , either as colloids or associated with Fe<sup>II</sup>-bearing mineral phases, which also act as catalysts for the Tc reduction.<sup>[2,3]</sup> Understanding the Tc redox processes in these conditions is essential for evaluating the safety of nuclear disposal sites; however, to date, even the structure of the  $\text{TcO}_2 \cdot x\text{H}_2\text{O}$  precipitates remains enigmatic and needs to be resolved.

Lukens et al.<sup>[4]</sup> proposed that  $\text{TcO}_2 \cdot x\text{H}_2\text{O}$  is formed by linear chains of equally spaced edge-sharing  $\text{TcO}_6$  octahedra with terminal  $\text{H}_2\text{O}$  ligands in the *trans* positions. In the same year, Vichot et al.<sup>[5]</sup> arrived at similar conclusions, but argued that the structure would alternate shorter and longer Tc–Tc distances along the chain, based on data available for  $\text{TcO}_2$  crystals.<sup>[6]</sup> However, these chain structures were based exclusively on EXAFS spectroscopy, which only provides radial interatomic distances and estimates of coordination numbers, and analogies to known crystal structures of other systems, like  $\text{CoCl}_2 \cdot 2\text{H}_2\text{O}$  and  $\text{RuO}_2 \cdot 2\text{H}_2\text{O}$ . In addition, in a recent work, Yalçintaş et al.<sup>[3a]</sup> showed that both the chain model with equally spaced Tc atoms (similar to the model by Lukens et al.<sup>[4]</sup>) and the one with alternating Tc–Tc distances (similar to crystalline  $\text{TcO}_2$ ) could describe equally well their own EXAFS

measurements of a fresh  $\text{TcO}_2 \cdot x\text{H}_2\text{O}$  precipitate, thereby demonstrating that a conclusive characterization of  $\text{TcO}_2 \cdot x\text{H}_2\text{O}$  based on EXAFS alone is impossible, even though EXAFS is, to the best of our knowledge, the only experimental technique applicable in this case due to the noncrystalline nature of  $\text{TcO}_2 \cdot x\text{H}_2\text{O}$ .

In this work, in order to unambiguously assign the  $\text{TcO}_2 \cdot x\text{H}_2\text{O}$  structure, we use density-functional theory (DFT) to obtain energetically viable structural models. The results from the DFT modeling are then used in the interpretation of EXAFS spectra of fresh and aged samples, showing that  $\text{TcO}_2 \cdot x\text{H}_2\text{O}$  precipitates are polymeric structures consisting of zigzag chains of  $\text{TcO}_6$  octahedra with  $\text{H}_2\text{O}$  groups in a *cis* configuration. In addition, we show that these polymeric chains eventually combine laterally, forming a tridimensional structure that might evolve to a new, low-energy  $\text{TcO}_2$  crystal phase.

## Results and Discussion

For the DFT modeling, our strategy was to derive infinite  $\text{TcO}_2 \cdot 2\text{H}_2\text{O}$  chains from  $\text{TcO}_2$  crystal structures constructed from the crystallographic coordinates of the three known  $\text{ReO}_2$  polymorphs, namely  $\alpha\text{-ReO}_2$  ( $P2_1/c$ ),<sup>[7]</sup>  $\beta\text{-ReO}_2$  ( $Pbcn$ ),<sup>[8]</sup> and  $\gamma\text{-ReO}_2$  ( $P4_2/mnm$ ).<sup>[9]</sup> Although only one  $\text{TcO}_2$  phase has been characterized experimentally (almost identical to  $\alpha\text{-ReO}_2$ ),<sup>[10]</sup> the use of  $\text{ReO}_2$  as initial reference is justifiable because Tc and Re have very similar crystal chemistry<sup>[11]</sup> and, thus,  $\text{TcO}_2$  counterparts of all  $\text{ReO}_2$  polymorphs should be expected to form. The corresponding  $\alpha$ -,  $\beta$ -, and  $\gamma$ - $\text{TcO}_2$  structures were obtained by replacing the Re atoms with Tc and performing full geometry optimizations, as described in the Experimental Section. Indeed, the optimized  $\text{TcO}_2$  structures turned out to be comparable to the  $\text{ReO}_2$  phases (Table S1 in the Supporting Information).

The calculated  $\text{TcO}_2$  crystal structures are represented in Figure 1a–c. All three polymorphs consist of edge-sharing  $\text{TcO}_6$  octahedra forming unidimensional chains that are laterally interconnected via corner-sharing O atoms. The chain configuration is characteristic of each  $\text{TcO}_2$  polymorph: in  $\alpha\text{-TcO}_2$ , the chains follow a straight path, with consecutive Tc–Tc pairs alternating between shorter and longer distances; the chains in  $\gamma\text{-TcO}_2$  are also straight, but the Tc atoms are separated by identical distances; in  $\beta\text{-TcO}_2$ , consecutive Tc atoms are also separated by identical distances, but the chains follow a distinctive zigzag path. From each  $\text{TcO}_2$  crystal structure, we extracted a single chain and converted the terminal O atoms into  $\text{H}_2\text{O}$  groups to balance the total electric charge, resulting in the  $\text{TcO}_2 \cdot 2\text{H}_2\text{O}$  chains shown in Figure S2a–c. We refer to these chains as  $\alpha$ -,  $\beta$ -, and  $\gamma$ - $\text{TcO}_2 \cdot 2\text{H}_2\text{O}$ , to indicate that the chains were derived from the  $\alpha$ -,  $\beta$ -, and  $\gamma$ - $\text{TcO}_2$  crystal structures, respectively. We also considered hydroxide chains (Figure S2d–f) where all O atoms were converted into OH groups; however, these chains turned out to be energetically disfavored, as shown in Table S3.

All structures were fully optimized (lattice vectors and atomic coordinates) using AMS/BAND<sup>[12]</sup> with the PBE<sup>[13]</sup> density functional, scalar relativistic effects,<sup>[14]</sup> and numerical atomic orbitals (NAOs) augmented with a triple-zeta polarized (TZP) set of Slater-type basis functions. For the chains, D3 dispersion corrections<sup>[15]</sup> were also included. Further computational details are provided in the Experimental Section.

Figure 1d–f shows the optimized structures and relative energies calculated for the  $\text{TcO}_2 \cdot 2\text{H}_2\text{O}$  chains. The  $\beta\text{-TcO}_2 \cdot 2\text{H}_2\text{O}$  structure (zigzag) is clearly the energetically most favored one; the energy difference to the next structure,  $\alpha\text{-TcO}_2 \cdot 2\text{H}_2\text{O}$ , is already significantly high (29.4 kJ mol<sup>−1</sup> per formula unit). Note that, whereas  $\beta$ - and  $\gamma$ - $\text{TcO}_2 \cdot 2\text{H}_2\text{O}$  retained their general structure,  $\alpha\text{-TcO}_2 \cdot 2\text{H}_2\text{O}$  rearranged into an oxyhydroxide chain,

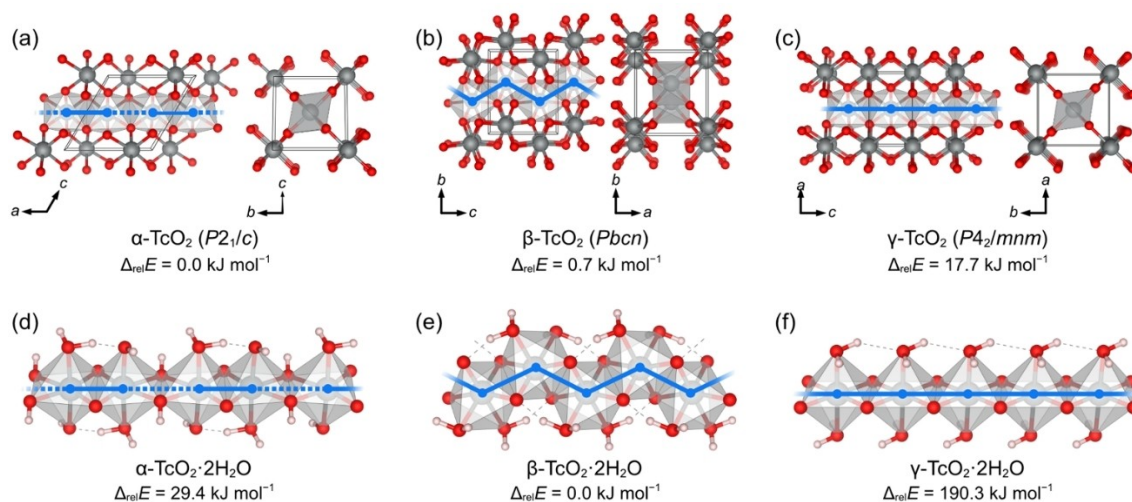


**Figure 1.**  $\text{TcO}_2$  crystal polymorphs and the  $\text{TcO}_2 \cdot 2\text{H}_2\text{O}$  infinite chains derived therefrom. Tc atoms represented as octahedra emphasize the structure of laterally interconnected chains in the  $\text{TcO}_2$  crystals, and the primitive unit cells are indicated by black lines. The blue lines emphasize the linear and zigzag paths of the chains, with dashed lines indicating the longer Tc–Tc distances (in the case of alternating long and short distances). The  $\text{TcO}_2$  crystals and  $\text{TcO}_2 \cdot 2\text{H}_2\text{O}$  chains were fully optimized with DFT. During the  $\alpha\text{-TcO}_2 \cdot 2\text{H}_2\text{O}$  optimization, a few H atoms migrated from the  $\text{H}_2\text{O}$  groups to  $\mu\text{-O}$  bridges. The relative energies per formula unit ( $\Delta_{\text{rel}}E$ ) of the optimized structures are shown.

which can be represented as  $Tc(\mu-O)(\mu-OH)(OH)(H_2O)$ ; nonetheless, for convenience, we will continue referring to this structure as  $\alpha-TcO_2 \cdot 2H_2O$ .

The Tc–O bond lengths as well as Tc–Tc distances calculated for the optimized  $TcO_2 \cdot 2H_2O$  chains are shown in Table 1 in comparison with the corresponding parameters obtained for the  $TcO_2$  crystal structures and from EXAFS spectra. The EXAFS parameters were determined by shell fitting (for details see the Supporting Information) from experimental spectra of a *fresh* and an *aged* sample. The spectrum of the fresh sample is the one published by Yalçintaş et al.,<sup>[3a]</sup> measured within a month after sample preparation; the shell fitting was redone in this work. The spectrum of the aged sample, on the other hand, is presented in this work for the first time; in this case, the  $TcO_2 \cdot xH_2O$  precipitate was stored in air, at room temperature, for about four years prior to the EXAFS measurement. The experimental EXAFS spectra of both samples were obtained at the Rossendorf Beamline at ESRF,<sup>[16]</sup> under identical conditions, most importantly, by using a closed-cycle He cryostat to maintain a temperature of 15 K and anoxic conditions during the measurement. They are shown in Figure 2, in comparison with the simulated spectra of the  $TcO_2 \cdot 2H_2O$  chains and  $TcO_2$  crystals calculated with DFT.

Table 1 clearly shows that, while the Tc–O bond lengths are characteristic of the chemical groups attached to the Tc atoms ( $\mu-O$ , O,  $\mu-OH$ , OH, and  $H_2O$ ), the Tc–Tc distances have characteristic values for each system, even if only the nearest Tc–Tc neighbors are considered. Thus, these systems would be clearly identifiable by EXAFS measurements. Note that the  $TcO_2 \cdot 2H_2O$  chains keep the same general characteristics of the  $TcO_2$  crystal structures, that is,  $\alpha$ - and  $\gamma$ - $TcO_2 \cdot 2H_2O$  form a straight chain, with alternating shorter and longer Tc–Tc distances in the former and only one Tc–Tc distance in the latter. Similarly,  $\beta$ - $TcO_2 \cdot 2H_2O$  – the energetically favored structure – remains as a zigzag chain with practically identical Tc–Tc distances.

The EXAFS Tc–O and Tc–Tc nearest-neighbor distances from the fresh and aged samples are in very good agreement

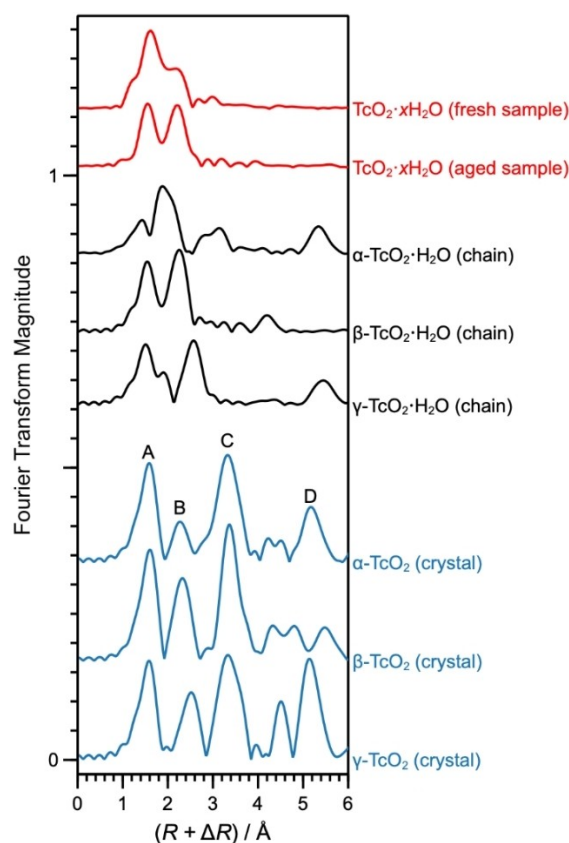


**Figure 2.** Fourier-transform magnitudes (FTMs) from experimental EXAFS spectra of the fresh and aged  $TcO_2 \cdot xH_2O$  precipitates (red curves) and from EXAFS spectra simulated with FEFF9.6.4<sup>[17]</sup> for the  $TcO_2 \cdot H_2O$  infinite chains (black curves) and  $TcO_2$  crystal structures (blue curves) optimized with DFT. The fresh sample was measured within a month of preparation;<sup>[3a]</sup> the aged sample was stored for four years under room conditions prior to measurement. The geometry of  $\alpha$ - $TcO_2 \cdot H_2O$  converged to a mixed protonation state, as shown in Figure 1d). For the  $TcO_2$  crystals, peak A is associated with the first Tc–O coordination shell, B with the nearest intrachain Tc–Tc neighbors, C with the nearest interchain Tc–Tc neighbors, and D with the second intrachain Tc–Tc neighbors.

**Table 1.** Tc coordination numbers (CN) and interatomic distances ( $R$ ) from EXAFS shell fitting of fresh and aged  $TcO_2 \cdot xH_2O$  samples along with the values obtained from DFT for the  $TcO_2 \cdot 2H_2O$  chains and  $TcO_2$  crystals. The CN values for the Tc–Tc interchain distances consider only one neighboring chain.

Shell	Exptl. EXAFS (shell fitting) $TcO_2 \cdot xH_2O$ precipitates				DFT calculations Infinite chains					Crystal structures						
	Fresh <sup>[a]</sup>		Aged <sup>[b]</sup>		$\alpha$ - $TcO_2 \cdot 2H_2O$ <sup>[c]</sup>		$\beta$ - $TcO_2 \cdot 2H_2O$		$\gamma$ - $TcO_2 \cdot 2H_2O$		$\alpha$ - $TcO_2$		$\beta$ - $TcO_2$		$\gamma$ - $TcO_2$	
	CN	R/Å	CN	R/Å	CN	R/Å	CN	R/Å	CN	R/Å	CN	R/Å	CN	R/Å	CN	R/Å
Tc–( $\mu$ -O)	4 <sup>[f]</sup>	2.01	4 <sup>[f]</sup>	2.01	2	1.93	4	1.98	4	1.97	6	2.01	6	2.01	6	2.00
Tc–OH <sub>2</sub>	2 <sup>[f]</sup>	2.39	2 <sup>[f]</sup>	2.14	1	2.11 <sup>[d]</sup>	2	2.23	2	2.24	–	–	–	–	–	–
Tc–Tc (intrachain)	2 <sup>[f]</sup>	2.55	2 <sup>[f]</sup>	2.54	1	2.34	2	2.53	2	2.90	1	2.62	2	2.64	2	2.84
			0.6	4.63	1	3.38	2	4.60	2	5.80	1	3.12	2	4.71	2	5.68
			4.2	7.03	2	5.71	2	6.98	2	8.70	2	5.73	2	7.16	2	8.53
Tc–Tc (interchain)	–	–	0.8	3.80	–	–	–	–	–	–	2	3.68	2	3.72	2	3.68
			1.2	5.06							1	5.24	2	5.26	2	5.46
			2.5	6.04							1	5.44	2	6.00	2	7.88

Errors of  $\pm 25\%$  are generally associated to CN values from EXAFS fitting. [a] Sample measured within a month from preparation.<sup>[3a]</sup> [b] Sample measured after four years of storage at room conditions. [c] Structure converged to an oxyhydroxide chain (Figure 1d). [d] OH bridge. [e] Terminal OH group. [f] Fixed during fitting.

with the distances in the calculated  $\beta\text{-TcO}_2\cdot 2\text{H}_2\text{O}$  chain, as shown in Table 1. The Tc–Tc distances (which characterize the chain structure) differ by  $\leq 0.02$  Å, whereas the Tc–( $\mu$ -O) bonds differ by  $\leq 0.03$  Å; the differences are slightly larger for the Tc–OH<sub>2</sub> bonds (0.16 Å for the fresh sample and 0.09 Å for the aged sample), but still in good agreement in both cases. The discrepancy between Tc–OH<sub>2</sub> bonds in the fresh and aged samples is reflected in the sharper splitting of the Fourier transform magnitude (FTM) peaks corresponding to the nearest Tc–O and Tc–Tc distances (peaks A and B in Figure 2). The most significant difference between the fresh and aged samples, however, is the absence of signals related to the longer Tc–Tc distances in the former, either because of a high static disorder of the chains or because the chains are too short to show such backscattering pairs consistently (note that thermal disorder can be excluded since both the fresh and the aged samples were measured at 15 K).

The most conclusive proof of the formation of zigzag chains in the  $\text{TcO}_2\cdot x\text{H}_2\text{O}$  precipitates comes from the EXAFS analysis of the aged sample. As shown in Figure 3, the  $\chi(k)$  spectrum of the aged precipitate contains high-frequency signals between 5 and 7 Å<sup>-1</sup> that are absent in the spectrum of the fresh sample. These signals correspond to second and third intrachain Tc–Tc distances of 4.63 and 7.03 Å shown in Table 1, which are only possible in the  $\beta\text{-TcO}_2\cdot 2\text{H}_2\text{O}$  chain (calculated as 4.71 and 7.16 Å). Interestingly, Tc–Tc distances of 3.80, 5.06, and 6.04 Å, corresponding to the interchain distances observed in the  $\beta\text{-TcO}_2$  crystal, could also be fitted, indicating that the precipitate develops a tridimensional organization with aging (Figure 4). Nonetheless, in the sample analyzed here, this tridimensional structure is likely in its initial stage, otherwise the EXAFS spectrum would bear a stronger resemblance to the spectrum of the  $\beta\text{-TcO}_2$  crystal in Figure 2, especially with respect to peak C.

The absence of interpretable EXAFS signals related to longer Tc–Tc distances in the fresh sample and the presence of the signals associated with long, interconnected parallel chains in the aged sample is indicative of the aging process in  $\text{TcO}_2\cdot x\text{H}_2\text{O}$  precipitates. In our interpretation, the short  $\beta\text{-TcO}_2\cdot 2\text{H}_2\text{O}$  chains combine with each other to form longer zigzag chains via condensation reactions, thereby releasing H<sub>2</sub>O. As the chains become longer, condensation reactions leading to cross-linked chains start to take place. The shortening of the second Tc–O path in the experimental EXAFS (denoted Tc–OH<sub>2</sub> in Table 1) from 2.39 Å in the fresh to 2.14 Å in the aged sample is an additional indication of this condensation process. This scenario is consistent with the thermodynamic evidence compiled by Grambow<sup>[18]</sup> that  $\text{TcO}_2\cdot x\text{H}_2\text{O}$  would release H<sub>2</sub>O over time and that the process takes place very slowly; as discussed above, after four years the aged sample still shows early signs of cross-linking between chains.

## Conclusion

In conclusion, by combining DFT calculations with EXAFS measurements, we have demonstrated that, contrary to the

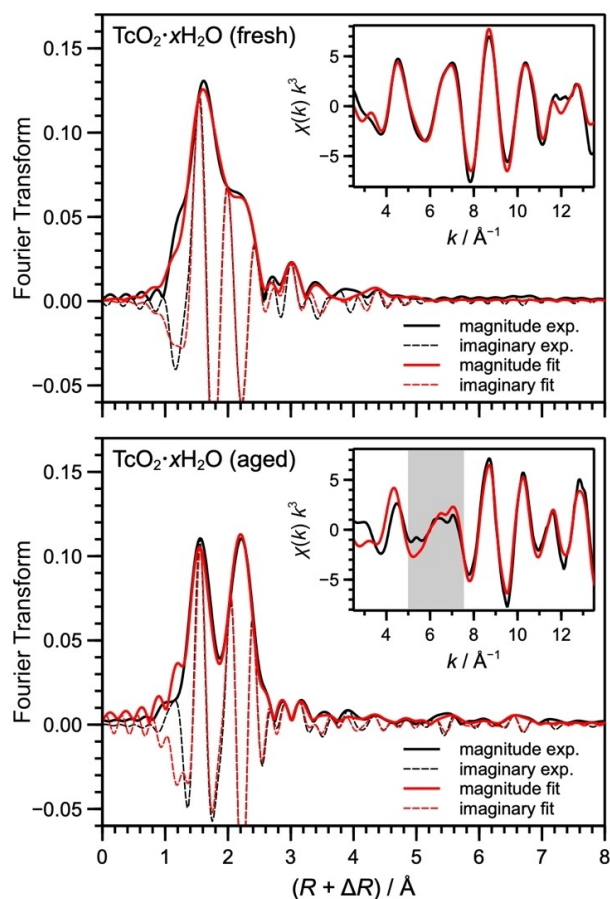


**Figure 3.** Experimental EXAFS spectra of fresh (top) and aged (bottom)  $\text{TcO}_2\cdot x\text{H}_2\text{O}$  samples (black traces) and their reproduction by shell fitting (red traces). The main plots show the Fourier transform magnitude (bold lines) and the imaginary part (thin lines); the inserts show the corresponding  $k^2$ -weighted  $\chi$  spectra (the shadowed region indicates high-frequency signals absent in the fresh sample). The shell fit of the fresh sample is based on the DFT-derived structure of  $\beta\text{-TcO}_2\cdot \text{H}_2\text{O}$  chain, the shell fit of the aged sample is based on the DFT-derived structure of the  $\beta\text{-TcO}_2$  crystal. The fitted parameters are compiled in Tables 1 and S4.

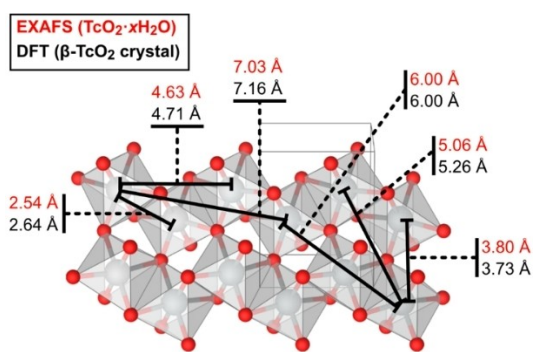


**Figure 4.** Intra- and interchain Tc–Tc distances. The DFT values (black) correspond to the optimized  $\beta\text{-TcO}_2$  crystal structure, whereas the EXAFS values (red) were obtained from fitting the experimental spectrum of the aged  $\text{TcO}_2\cdot x\text{H}_2\text{O}$  sample.

currently anticipated linear structure,  $\text{TcO}_2\cdot x\text{H}_2\text{O}$  precipitates are polymeric structures formed of zigzag chains of edge-

sharing  $\text{TcO}_6$  octahedra with terminal  $\text{H}_2\text{O}$  ligands at the *cis* positions (Figure 1e). Differences in the EXAFS of a fresh sample and a sample aged for four years indicate that the length of the polymeric chains increases slowly over time and might lead to crystallization of a yet uncharacterized  $\text{TcO}_2$  phase analogous to  $\beta\text{-ReO}_2$  (Figure 1b), which our calculations (Table S2) show to be energetically equivalent to the known  $P2_1/c^{[10]}$  ( $\alpha\text{-TcO}_2$ ) phase.

## Experimental Section

### DFT calculations

***TcO<sub>2</sub> and ReO<sub>2</sub> crystal structures:*** The initial  $\text{TcO}_2$  and  $\text{ReO}_2$  structures were constructed from crystallographic data for  $\alpha\text{-ReO}_2^{[7]}$  (monoclinic,  $P2_1/c$ ),  $\beta\text{-ReO}_2^{[8]}$  (orthorhombic,  $Pbcn$ ), and  $\gamma\text{-ReO}_2^{[9]}$  (tetragonal,  $P4_2/mnm$ ), depicted in Figure S1. The equivalent  $\text{TcO}_2$  structures were obtained simply by replacing the Re atoms with Tc. Finally, the tetragonal phases ( $\gamma\text{-TcO}_2$  and  $\gamma\text{-ReO}_2$ ) were duplicated in the *c* direction ( $1 \times 1 \times 2$  supercells), so that all cells would contain four  $\text{TcO}_2$  or  $\text{ReO}_2$  formula units. Subsequently, the atomic coordinates and lattice vectors were fully optimized using the PBE<sup>[13]</sup> density functional with numerical atomic orbitals (NAOs) augmented with a triple-zeta polarized (TZP) set of Slater-type basis functions; relativistic effects were included by using the zeroth-order regular approximation (ZORA).<sup>[14]</sup> These calculations were conducted with the AMS/BAND<sup>[12]</sup> program, using regular *k*-space grids with quality set to “Good” and default convergence criteria.

***TcO<sub>2</sub>·2H<sub>2</sub>O infinite chains:*** The initial  $\text{TcO}_2 \cdot 2\text{H}_2\text{O}$  chains were constructed by extracting a single chain of edge-sharing  $\text{TcO}_6$  octahedra from each  $\text{TcO}_2$  crystal phase and saturating the O atoms with H according to two approaches, as shown in Figure S2: (a–c) terminal O atoms were converted into  $\text{H}_2\text{O}$  ligands and bridging O atoms were left unprotonated, resulting in  $(\text{Tc}(\mu\text{-O})_2(\text{OH})_2)_n$  chains; (d–f) terminal and bridging O atoms were converted into OH groups, resulting in  $(\text{Tc}(\text{OH})_2(\mu\text{-OH})_2)_n$  chains. Finally, the atomic coordinates and lattice parameter of each structure were fully optimized using the method described above for the crystal structures, supplemented with Grimme’s D3 corrections<sup>[15]</sup> to improve the description of dispersion interactions with OH and  $\text{H}_2\text{O}$  groups. Like for the crystal structures, these calculations were conducted with the AMS/BAND<sup>[12]</sup> program, using regular *k*-space grids with quality set to “Good”. Note that these systems are periodic only along the chain direction.

***Single-point calculations:*** Energies and electronic properties were calculated for the optimized structures with the same methods used in the preceding geometry optimizations, except for a denser *k*-space grid (quality set to “VeryGood”). For comparison, single-point calculations were also carried out within the FHI-aims program,<sup>[19]</sup> using the PBE<sup>[13]</sup> and HSE06<sup>[20]</sup> density functionals with a “tier 1” set of atom-centered NAO basis functions; relativistic effects were described with the “atomic ZORA” approach,<sup>[19]</sup> for the  $\text{TcO}_2 \cdot 2\text{H}_2\text{O}$  infinite chains, the Tkatchenko-Scheffler (TS) method<sup>[21]</sup> was used for the dispersion interactions.

### TcO<sub>2</sub>·xH<sub>2</sub>O samples and EXAFS measurements

***Fresh sample:*** The preparation and EXAFS spectrum of the fresh sample were reported by Yalçintaş et al.<sup>[3a]</sup> The  $\text{TcO}_2 \cdot x\text{H}_2\text{O}$  precipitate was prepared by acidifying a pertechnetate solution with concentrated HCl, then adding Zn to generate nascent hydrogen. After the reaction was completed, NaOH (20 M) was added to obtain a black precipitate, which aged for one week. The sample

was stored under Ar at liquid nitrogen temperature. The EXAFS was measured within 30 days of preparation at the Rossendorf Beamline (BM20 at ESRF, Grenoble, France) in fluorescence mode at the Tc K-edge (21044 eV). The sample was kept at 15 K during the measurement. Further details can be found in the original publication.<sup>[3a]</sup>

***Aged sample:*** The sample was prepared by hydrolysis of  $\text{K}_2[\text{TcCl}_6]$ , which was previously synthesized by an established procedure.<sup>[22]</sup> Solid  $\text{K}_2[\text{TcCl}_6]$  (390 mg, 1 mmol) was dissolved in 0.5 mL  $\text{H}_2\text{O}$ , which resulted in the precipitation of a dark brown solid. An aqueous solution of KOH (2 mL, 0.1 M) was added, and the suspension was stirred for 5 h at room temperature. The formed black brown solid was filtered off and washed with water ( $5 \times 1$  mL). The absence of  $\text{Cl}^-$  in the final washing solution was checked by the addition of  $\text{Ag}(\text{NO}_3)$ . The thus formed  $\text{TcO}_2 \cdot x\text{H}_2\text{O}$  was dried in air at room temperature. Yield: practically quantitative. The sample was prepared and stored at room temperature in air for four years prior to the EXAFS measurement, which was conducted identically to the fresh sample.

### EXAFS analyses

***EXAFS shell fitting:*** Tc K-edge EXAFS shell fittings were conducted in R-space with WinXAS<sup>[23]</sup> using the  $\beta\text{-TcO}_2 \cdot 2\text{H}_2\text{O}$  chain structure optimized with DFT (Figure 2e) for the oxygen coordination to Tc and for intrachain Tc–Tc distances. Interchain Tc–Tc distances from the DFT-derived  $\beta\text{-TcO}_2$  crystal structure were also included. The spectrum of the fresh precipitate was well fit by four oxygen atoms at 2.01 Å and two oxygen atoms at 2.39 Å, and 8 additional four-legged multiple scattering paths arising from the quasi square-planar configuration of the four nearest oxygen atoms (Table S4). Furthermore, we obtained two Tc atoms at 2.55 Å. These radial distances are in excellent agreement with the local structure of  $\beta\text{-TcO}_2 \cdot 2\text{H}_2\text{O}$ , except for the two longer Tc–O distances, which represent the two water molecules in the coordination sphere and are about 0.2 Å longer than predicted by DFT. Note that a similarly long distance has been determined by Lukens et al.,<sup>[4]</sup> also by EXAFS shell fitting. The spectrum of the fresh precipitate does not reveal any backscattering peaks at longer Tc–Tc distances that could be fitted. For the aged sample, in addition to the local structure obtained for the fresh sample, Tc–Tc distances corresponding to the 2nd and 3rd intrachain shells and for the three interchain shells (Figure 4) could also be fitted (Table S4 and Figure 3), in good agreement with the parameters in the  $\beta\text{-TcO}_2 \cdot 2\text{H}_2\text{O}$  chain and  $\beta\text{-TcO}_2$  crystal. The amplitude reduction factor  $S_0^2$  was fixed to 0.8 for all fits.

***EXAFS simulation:*** EXAFS spectra were simulated for the DFT-optimized structures with the program FEFF9.6.4<sup>[17]</sup> using the self-consistent field mode with a global Debye-Waller factor of 0.003 Å, amplitude reduction factor of 0.9, and  $\Delta E_0 = 0$ .

## Acknowledgements

The research was funded by the European Commission (EC) through the EURAD FUTURE T3 project (H2020-847593) and by the German Federal Ministry of Education and Research (BMBF) through the KRIMI project (02NUK056C). The authors also thank Prof. Bernd Grambow (SUBATECH Nantes, France) for fruitful discussions. Open Access funding enabled and organized by Projekt DEAL.

## Conflict of Interest

The authors declare no conflict of interest.

## Data Availability Statement

The data that support the findings of this study are available in the supplementary material of this article.

**Keywords:** chain structures · density functional calculations · EXAFS spectroscopy · nuclear waste management · technetium

- [1] R. Alberto, *COSMOS* **2012**, *8*, 83.
- [2] J. P. Icenhower, N. P. Qafoku, J. M. Zachara, W. J. Martin, *Am. J. Sci.* **2010**, *310*, 721.
- [3] a) E. Yalçintaş, A. C. Scheinost, X. Gaona, M. Altmaier, *Dalton Trans.* **2016**, *45*, 17874; b) K. Morris, F. R. Livens, J. M. Charnock, I. T. Burke, J. M. McBeth, J. D. C. Begg, C. Boothman, J. R. Lloyd, *Appl. Geochem.* **2008**, *23*, 603; c) T. S. Peretyazhko, J. M. Zachara, R. K. Kukkadapu, S. M. Heald, I. V. Kutnyakov, C. T. Resch, B. W. Arey, C. M. Wang, L. Kovarik, J. L. Phillips, D. A. Moore, *Geochim. Cosmochim. Acta* **2012**, *92*, 48; d) J. M. McBeth, J. R. Lloyd, G. T. W. Law, F. R. Livens, I. T. Burke, K. Morris, *Mineral. Mag.* **2011**, *75*, 2419.
- [4] W. W. Lukens, J. J. Bucher, N. M. Edelstein, D. K. Shuh, *Environ. Sci. Technol.* **2002**, *36*, 1124.
- [5] L. Vichot, G. Ouvrard, G. Montavon, M. Fattahi, C. Musikas, B. Grambow, *Radiochim. Acta* **2002**, *90*, 575.
- [6] I. Almahamid, J. C. Bryan, J. J. Bucher, A. K. Burrell, N. M. Edelstein, E. A. Hudson, N. Kaltsoyannis, W. W. Lukens, D. K. Shuh, H. Nitsche, T. Reich, *Inorg. Chem.* **1995**, *34*, 193.
- [7] F. F. Ferreira, H. P. S. Correa, M. T. D. Orlando, J. L. Passamai Jr., C. G. P. Orlando, I. P. Cavalcante, F. Garcia, E. Tamura, L. G. Martinez, J. L. Rossi, F. C. L. de Melo, *J. Synchrotron Radiat.* **2009**, *16*, 48.
- [8] A. Magnéli, *Acta Chem. Scand.* **1957**, *11*, 28.
- [9] A. L. Ivanovskii, T. I. Chupakhina, V. G. Zubkov, A. P. Tyutyunnik, V. N. Krasilnikov, G. V. Bazuev, S. V. Okatov, A. I. Lichtenstein, *Phys. Lett. A* **2005**, *348*, 66.
- [10] E. E. Rodriguez, F. Poineau, A. Llobet, A. P. Sattelberger, J. Bhattacharjee, U. V. Waghmare, T. Hartmann, A. K. Cheetham, *J. Am. Chem. Soc.* **2007**, *129*, 10244.
- [11] a) S. Duckworth, X. Gaona, D. Castaño, S. Park, M. Altmaier, H. Geckeis, *Appl. Geochem.* **2021**, 105037; b) P. V. Grundler, L. Helm, R. Alberto, A. E. Merbach, *Inorg. Chem.* **2006**, *45*, 10378.
- [12] a) G. te Velde, E. J. Baerends, J. A. Berger, P. L. d. Boeij, M. Franchini, J. A. Groeneveld, E. S. Kadantsev, R. Klooster, F. Kootstra, P. Romaniello, M. Raupach, D. G. Skachkov, J. G. Snijders, C. J. O. Verzijl, J. A. C. Gil, J. M. Thijssen, G. Wiesenekker, C. A. Peeples, G. Schreckenbach, T. Ziegler, BAND2019, SCM, Theoretical Chemistry, Vrije Universiteit, Amsterdam, The Netherlands, **2019**; c) R. Rüger, M. Franchini, T. Trnka, A. Yakovlev, E. v. Lenthe, P. Philipsen, B. Klumpers, T. Soini, AMS 2019, SCM, Theoretical Chemistry, Vrije Universiteit, Amsterdam, The Netherlands, **2019**.
- [13] J. P. Perdew, K. Burke, M. Ernzerhof, *Phys. Rev. Lett.* **1996**, *77*, 3865.
- [14] P. H. T. Philipsen, E. vanLenthe, J. G. Snijders, E. J. Baerends, *Phys. Rev. B* **1997**, *56*, 13556.
- [15] S. Grimme, J. Antony, S. Ehrlich, H. Krieg, *J. Chem. Phys.* **2010**, *132*, 154104.
- [16] A. C. Scheinost, J. Claussner, J. Exner, M. Feig, S. Findeisen, C. Hennig, K. O. Kvashnina, D. Naudet, D. Prieur, A. Rossberg, M. Schmidt, C. Qiu, P. Colomp, C. Cohen, E. Dettona, V. Dyadkin, T. Stumpf, *J. Synchrotron Radiat.* **2021**, *28*, 333.
- [17] a) J. J. Rehr, R. C. Albers, *Rev. Mod. Phys.* **2000**, *72*, 621; b) J. J. Rehr, J. J. Kas, M. P. Prange, A. P. Sorini, Y. Takimoto, F. Vila, *C. R. Phys.* **2009**, *10*, 548; c) J. J. Rehr, J. J. Kas, F. D. Vila, M. P. Prange, K. Jorissen, *Phys. Chem. Chem. Phys.* **2010**, *12*, 5503.
- [18] I. Grenthe, X. Gaona, L. Rao, A. Plyasunov, W. Runde, B. Grambow, R. Konings, A. Smith, E. Moore, M.-E. Ragoussi, J. S. Martinez, D. Costa, A. Felmy, K. Spahiu, *Second Update on the Chemical Thermodynamics of Uranium, Neptunium, Plutonium, Americium and Technetium, Vol. 14*, Nuclear Energy Agency of the OECD (NEA), **2021**.
- [19] V. Blum, R. Gehrke, F. Hanke, P. Havu, V. Havu, X. Ren, K. Reuter, M. Scheffler, *Comput. Phys. Commun.* **2009**, *180*, 2175.
- [20] a) J. Heyd, G. E. Scuseria, M. Ernzerhof, *J. Chem. Phys.* **2003**, *118*, 8207; b) J. Heyd, G. E. Scuseria, M. Ernzerhof, *J. Chem. Phys.* **2006**, *124*, 219906; c) A. V. Krukau, O. A. Vydrov, A. F. Izmaylov, G. E. Scuseria, *J. Chem. Phys.* **2006**, *125*, 224106.
- [21] A. Tkatchenko, M. Scheffler, *Phys. Rev. Lett.* **2008**, *102*, 073005.
- [22] K. Schwochau in *Handbuch der Präparativen Anorganischen Chemie, Vol. 3* (Ed.: G. Brauer), Stuttgart, **1981**, pp. 1597.
- [23] T. Ressler, *J. Synchrotron Radiat.* **1998**, *5*, 118.

Manuscript received: July 20, 2022

Accepted manuscript online: September 2, 2022

Version of record online: September 23, 2022